Check for updates

ADVANCING EARTH AND SPACE SCIENCES

Geophysical Research Letters

RESEARCH LETTER
10.1029/2024GL112886

The Dominant Source Mechanism of Infrasound Generation in Powder Snow Avalanches

B. Sovilla[1], E. Marchetti[2], M. L. Kyburz[1,3,4], A. Köhler[5], P. Huguenin[1], I. Calic[1], M. J. Kohler[1], E. Suriñach[6], and C. Pérez-Guillén[1]

[1]WSL Institute for Snow and Avalanche Research SLF, Davos, Switzerland, [2]Department of Earth Sciences, University of Firenze, Firenze, Italy, [3]Chair of Alpine Mass Movements, ETH Zürich, Zürich, Switzerland, [4]Climate Change, Extremes, and Natural Hazards in Alpine Regions Research Centre CERC, Davos, Switzerland, [5]Department for Natural Hazards, Austrian Research Centre for Forests, Innsbruck, Austria, [6]Geomodels and Earth Sciences Faculty, RISKNAT Avalanches Research Group, University of Barcelona, Barcelona, Spain

Key Points:

- Particle clusters suspended in the airborne layers of powder snow avalanches (PSAs) are the dominant source of infrasound
- Infrasound from PSAs originates from a distributed source, extending up to hundreds of meters behind the avalanche front
- Infrasound from PSAs is proportional to the kinetic energy of the particle clusters in suspension

Supporting Information:

Supporting Information may be found in the online version of this article.

Correspondence to:

B. Sovilla,
sovilla@slf.ch

Citation:

Sovilla, B., Marchetti, E., Kyburz, M. L., Köhler, A., Huguenin, P., Calic, I., et al. (2025). The Dominant source mechanism of infrasound generation in powder snow avalanches. *Geophysical Research Letters*, *52*, e2024GL112886. https://doi.org/10.1029/2024GL112886

Received 2 OCT 2024
Accepted 12 DEC 2024

Author Contributions:

Conceptualization: B. Sovilla, E. Marchetti
Data curation: B. Sovilla, M. L. Kyburz, A. Köhler, P. Huguenin, I. Calic, M. J. Kohler, E. Suriñach, C. Pérez-Guillén
Formal analysis: B. Sovilla, M. L. Kyburz
Funding acquisition: B. Sovilla, E. Suriñach
Investigation: B. Sovilla, M. L. Kyburz, P. Huguenin
Methodology: B. Sovilla, E. Marchetti, M. L. Kyburz, C. Pérez-Guillén
Visualization: B. Sovilla, P. Huguenin
Writing – original draft: B. Sovilla, E. Marchetti

© 2025. The Author(s).
This is an open access article under the terms of the Creative Commons Attribution-NonCommercial-NoDerivs License, which permits use and distribution in any medium, provided the original work is properly cited, the use is non-commercial and no modifications or adaptations are made.

Abstract Powder snow avalanches (PSAs) radiate infrasound energy, yet the source mechanism remains unclear, limiting hazard monitoring and mitigation with infrasound-based technologies. Here, we analyze a unique data set from a large PSA to improve the understanding of the source mechanism. Through comparison of cluster activity within the airborne layers of the PSA and the recorded infrasound signal in the frequency domain, we demonstrate that infrasound is mainly generated from particle clusters suspended by turbulent eddies or ejected from the denser basal layer. Further correlating infrasound amplitudes with radar-derived spatial distributions of these clusters, we reveal a distributed source extending hundreds of meters behind the avalanche front. Additionally, we establish a relationship between infrasound and kinetic energy of suspended particles. These findings deepen our understanding of the complex dynamics of infrasound generation, offering valuable insights for avalanche detection and early warning strategies, and fundamental comprehension of PSA dynamics.

Plain Language Summary Powder snow avalanches (PSAs) generate low-frequency sound waves below the threshold of human hearing, called infrasound. Infrasound can travel long distances, which allows for simple and effective avalanche monitoring. However, it is unclear where and how infrasound is produced, limiting the use of infrasound detection systems for avalanche risk management. To address this, we analyze data from a large naturally occurring PSA. We match the activity of suspended snow particles in the airborne layers, captured by a high-speed camera, with the recorded infrasound. We show that infrasound may originate from particle clusters carried by turbulent eddies or expelled from the denser regions of the PSA. Using radar measurements, we map the spatial distribution of these clusters, revealing an infrasound source extending hundreds of meters behind the avalanche front. Furthermore, we find a connection between infrasound and the kinetic energy of suspended particles, offering a new approach to assess the destructive potential of PSAs. These findings deepen our understanding of infrasound generation during avalanches, providing crucial information for avalanche detection, early warning systems, and understanding the mechanisms behind PSA generation. Moreover, the findings could also be valuable for understanding and managing similar types of gravitational flows, such as pyroclastic surges during volcanic eruptions.

1. Introduction

Gravitational flows, such as snow avalanches, pyroclastic surges or debris flows, produce infrasound waves that propagate, with little dissipation, in the surrounding atmosphere. Consequently, infrasound is widely used to detect gravitational flows, offering an efficient technology for hazard mitigation (see Marchetti and Johnson (2023) for a review). Despite the success of this technology, the source of infrasound remains poorly understood, which limits more quantitative analyses.

In gravitational flows, it is hypothesized that infrasound originates from irregular and energetic material movements, generating air compressions and rarefactions that propagate as sound waves (Bedard et al., 1988; Naugolnykh & Bedard, 2002). Indeed, such flows frequently exhibit abrupt changes in velocity, density, and pressure. This has been observed in field studies at the Vallée de la Sionne full-scale avalanche test site (VdlS), where organized patterns of particle motion within turbulent airborne layers of powder snow avalanches (PSAs) generate pressure peaks due to their dynamic and fluctuating nature (Sovilla et al., 2018). Similar phenomena

19448007, 2025, 2, Downloaded from https://agupubs.onlinelibrary.wiley.com/doi/10.1029/2024GL112886 by CochraneAustria, Wiley Online Library on [13/01/2025]. See the Terms and Conditions (https://onlinelibrary.wiley.com/terms-and-conditions) on Wiley Online Library for rules of use; OA articles are governed by the applicable Creative Commons License

Writing – review & editing: M. L. Kyburz, A. Köhler, I. Calic, M. J. Kohler, C. Pérez-Guillén

have been observed in laboratory experiments of pyroclastic surges by Brosch et al. (2021), revealing energetic turbulent structures producing high-pressure pulses. Furthermore, waves and oscillations on the surface of debris flows are common and Belli et al. (2022) demonstrated their link to infrasound radiation.

Various snow avalanche studies, based on limited measurements of avalanche trajectory, front velocity, and visual observations, have linked this low-frequency sound to the presence of a well-developed snow powder cloud (Johnson et al., 2021; Kogelnig et al., 2011; Marchetti et al., 2020; Watson et al., 2022). However, these studies were inconclusive regarding the exact process responsible for infrasound generation, primarily due to the lack of measurements characterizing the turbulent, particle-laden layers. These layers include the faster intermittency layer, where particles in suspension are organized into large clusters, with densities up to 20 times greater than the surrounding gas-fine particle mixture, generating intermittent pressure peaks due to their dynamic and fluctuating nature. In contrast, the slower suspension layer, is where fine particles are more uniformly distributed in the velocity field and settling occurs. Both layers can extend for tens of meters in height and cover a dense basal layer, 0.5–2 m thick (Sovilla et al., 2018).

Recently, the installation of a high-speed camera at VdlS has provided unprecedented insights into one of the most elusive processes in PSAs: particle clustering within the airborne, turbulent regions. This new observation, combined with extensive measurements routinely performed at the site, offers unique benchmark data to identify the primary source responsible for infrasound generation in PSAs at field scale. In the following sections, we will illustrate how particle clusters and their spatial distribution contribute to infrasound generation.

2. Materials and Methods

The measurements were performed at VdlS (Figure 1), located in the canton of Valais in southwestern Switzerland. Measurements are triggered automatically when the amplitudes recorded by seismic sensors exceed a predefined threshold. All measuring devices are time-synchronized through an electrical pulse sent to the sensors when the acquisition system activates. Radars and an infrasound sensor are installed at the bottom of the slope and monitor the avalanche descent from release to deposit (Figure 1). Measurements of internal flow parameters such as velocity and pressure are performed on a 20 m high steel pylon. Since 2017, a high-speed camera is installed on the pylon and monitors particles flowing inside the intermittency and suspension layers (Figures S1–S2 in Supporting Information S1).

2.1. Infrasound Measurements

In VdlS, infrasound data has been acquired since 2008 (Kogelnig et al., 2011). The sensor (Chaparral Model 24, 0.1–200 Hz bandwidth) is located on the valley floor, close to the bunker (Figure 1), and records the signals emitted by the avalanche from the release, at a distance of up to 2.2 km, to the deposit. For large avalanches, the suspension and the intermittency layer occasionally overrun the sensor. At this short distance, sound propagation effects are negligible (Kogelnig et al., 2014; Marchetti & Johnson, 2023) and infrasound is mainly controlled by the source mechanism and its spatial extent, as well as interactions with the topography (McKenna et al., 2012). Throughout the winter season, infrasound data is collected at 100 Hz, both in continuous and VdlS trigger mode. The raw data is bandpass filtered from 0.1 to 50 Hz.

2.2. GEODAR and Doppler Radar

A few meters from the infrasound sensor, a pulse Doppler radar (Gauer et al., 2007) and a frequency modulated continuous wave radar, called GEODAR (Ash et al., 2010), monitor the avalanche descent from a bunker (Figure 1). Operating at approximately 5 GHz, these radars detect reflections from objects larger than about 5 cm. Signatures on GEODAR's Moving Target Identification (MTI) plots (Figure 2d), enable assessment of avalanche flow regimes, including the onset and decay of the intermittency regime (Köhler et al., 2018). In contrast to GEODAR, the Pulse-Doppler radar captures the full velocity spectrum of the avalanche. Due to the Doppler processing, however, it has a lower spatial resolution of 25 m compared to the sub-meter resolution of the GEODAR. Each pulse analyzed by the Doppler radar consists of 73 range gates. Doppler radar measurements are visualized similarly to the GEODAR's MTI plots (Figure 4), but show the velocity at maximum intensity V_{Imax}. V_{Imax} is commonly referred to as the material velocity, and represents the velocity at which most of the material within the radar sight is flowing (Gauer et al., 2007) (Text S1 and Figure S4 in Supporting Information S1).

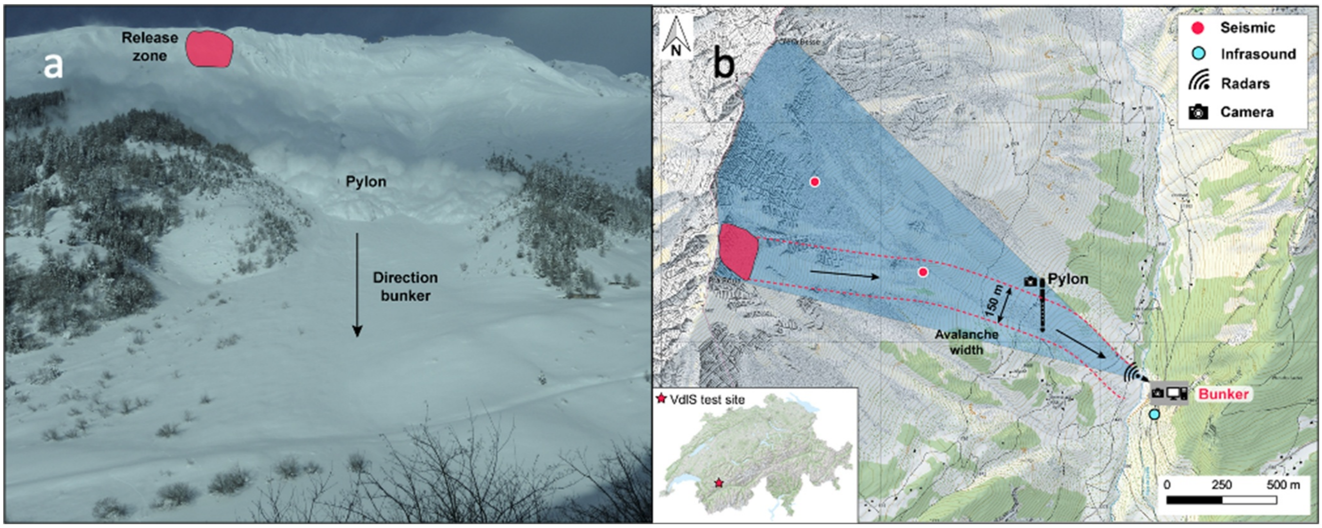

Figure 1. (a) Picture from the bunker during the descent of a powder snow avalanche at the VdlS. This avalanche was similar in size and release zone to the one studied in this paper, which unfortunately occurred at night. Radars and infrasound sensors are also installed in or near the bunker, providing measurements from the same viewing angle. The 20 m high pylon is barely visible, obscured by the intermittency and suspension layers, which cannot be visually distinguished. (b) The map shows the location of the instruments, the release zone (red area), and the VdlS monitored basin (blue area), along with the approximate width of the intermittency layer (red dashed lines).

2.3. High-Speed Camera Imaging

In the avalanche runout zone, 670 m air-line distance from the infrasound sensor and radars (Figure 2d, blue line), a high-speed camera mounted 14 m above the ground on the pylon records snow particles suspended in the intermittency and suspension layers (Figures 2a–2c). The images reveal a wide range of particle cluster sizes, which appear as bright spots due to their higher light reflectance compared to the surrounding air-snow crystals mixture. Due to the limited frame rate of 142 fps, the temporal resolution is insufficient to extract the velocity or size of individual particles. However, by extracting the average brightness of each image, it is possible to reconstruct the time series and thus the frequency of particle clustering. Hence, we consider brightness intensity as a proxy for particle concentration (Bernard & Wallace, 2002). The brightness for each image is obtained by averaging the values of 2,048 × 2,048 8-bit gray scale pixels with values ranging from 0 to 255 (Figure S6 in Supporting Information S1).

3. Data

The PSA analyzed in this study occurred on 15 January 2021, and was chosen for its exemplary data, which was collected simultaneously with the infrasound sensor, high-speed camera, GEODAR and Doppler radar (Fischer et al., 2024; Kyburz & Sovilla, 2024). This avalanche exhibited a significant intermittency zone with three surges and high velocities up to 100 s (Figure 2d). The intermittency layer was coupled with a thinner, slower-moving basal layer, approximately 0.5–1 m compared to the 10–20 m height of the intermittency zone. The basal layer only becomes visible after 100 s, as the substantial amount of suspended material impedes the radar from penetrating down to the dense basal layer within the intermittency zone.

The avalanche reached the location of the high-speed camera 53 s after the seismic trigger (Figures 2d and 2e). The high-speed camera recorded the entire avalanche passage, measuring inside the intermittency and suspension layers (Figures 2a–2e). The arrival of the avalanche at the pylon is marked by the sudden increase in the brightness data (Figure 2e). The signal between 53 and 100 s exhibits significant oscillations around a constant brightness level, indicating the passage of large particle clusters (Figures 2a and 2b) within a mixture of snow crystals and air with relatively constant density. These oscillations around the average level are caused by areas of substantial material transport, characterized by densification or clustering, immediately followed by areas with lower material transport, resulting in significantly lower average luminosity in the images. From 100 s, the brightness

19448007, 2025, 2, Downloaded from https://agupubs.onlinelibrary.wiley.com/doi/10.1029/2024GL112886 by CochraneAustria, Wiley Online Library on [13/01/2025]. See the Terms and Conditions (https://onlinelibrary.wiley.com/terms-and-conditions) on Wiley Online Library for rules of use; OA articles are governed by the applicable Creative Commons License

19448007, 2025, 2, Downloaded from https://agupubs.onlinelibrary.wiley.com/doi/10.1029/2024GL112886 by CochraneAustria, Wiley Online Library on [13/01/2025]. See the Terms and Conditions (https://onlinelibrary.wiley.com/terms-and-conditions) on Wiley Online Library for rules of use; OA articles are governed by the applicable Creative Commons License

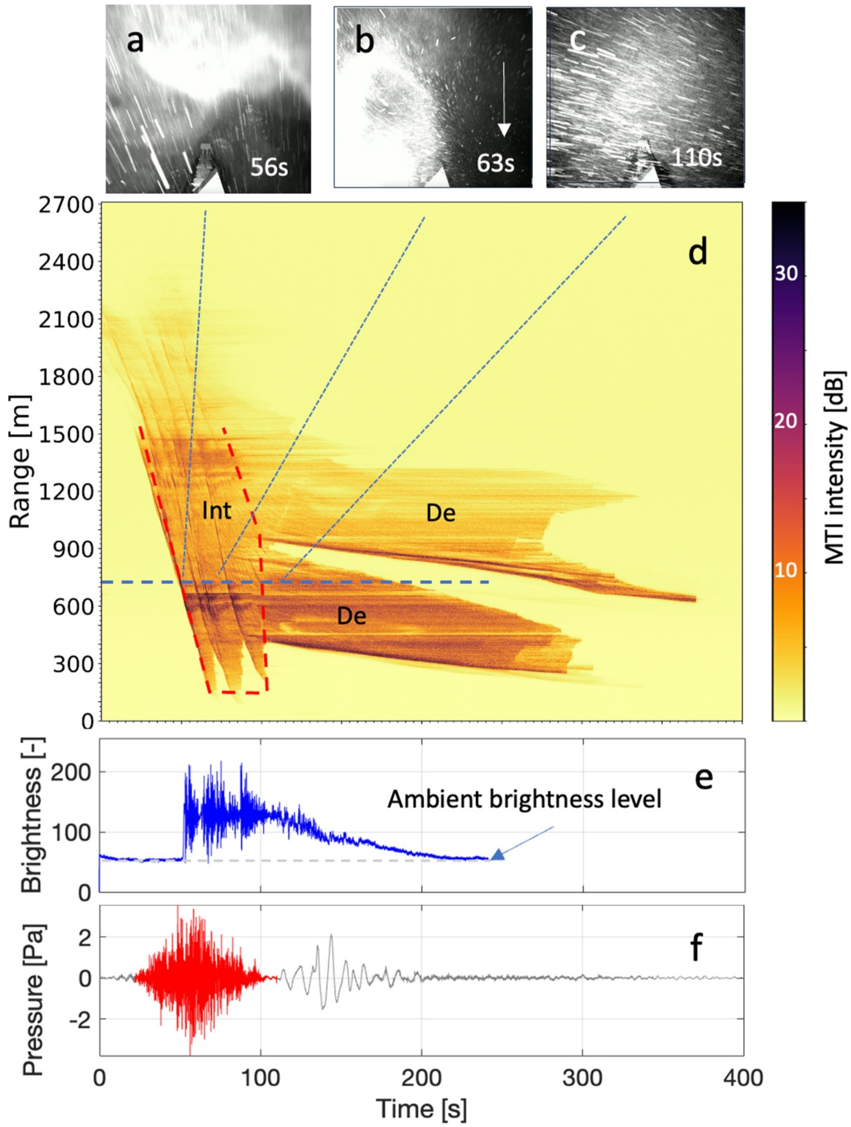

Figure 2. Particle clusters within the intermittency layer (a, b) and a view inside the suspension layer (c), captured by the high-speed camera installed on the pylon, 14 m above the ground (Figure 1). The main flow direction is indicated by an arrow. As a scale reference, the triangular shape at the bottom of the images is 60 cm wide. (d) GEODAR Moving Target Identification plot. The red dashed line highlights the intermittency zone (Int), showing a distinct signature compared to the dense layer (De). The horizontal blue dashed line denotes the position of the pylon and camera, with its length representing the duration of camera measurements. (e) Brightness extracted from high-speed camera images. (f) Infrasound signal. The red highlighted signal is generated by the intermittency layer. The data is time-synchronized.

amplitude decreases, indicating smaller clusters and particle settling (Figure 2c). The brightness level reaches the initial ambient value 220 s after the trigger, signaling the settlement of all suspended particles. By analyzing the time-synchronized data, we were able to distinguish the infrasound signal associated with the intermittency zone (highlighted in red in Figure 2f). The low-frequency signal observed between 100 and 200 s was likely produced by advection recorded at the infrasound sensor either generated by the air velocity field around the moving avalanche (Marchetti et al., 2021) or by the suspension layer reaching the sensor. The dense layer's infrasound contribution from 200 to 370 s was negligible compared to that of the intermittency zone (Figure S3 in Supporting Information S1).

19448007, 2025, 2, Downloaded from https://agupubs.onlinelibrary.wiley.com/doi/10.1029/2024GL112886 by CochraneAustria, Wiley Online Library on [13/01/2025]. See the Terms and Conditions (https://onlinelibrary.wiley.com/terms-and-conditions) on Wiley Online Library for rules of use; OA articles are governed by the applicable Creative Commons License

4. Results

4.1. The Source Process

The synchronization between infrasound and GEODAR measurements enables precise attribution of the dominant infrasound source to a specific PSA region, namely the intermittency region (Figures 2d and 2f). Other regions can be excluded as significant sources of infrasound through comparison in Figure 2: the dense layer (De) completely stops around 350 s (Figure 2d) and the suspension layer decays at around 220 s (Figure 2e).

The intermittency layer is a snow-laden turbulent flow where turbulent air interacts dynamically with suspended snow particles, mostly organized into particle clusters (Sovilla et al., 2018). Thus, this limits the potential infrasound source mechanisms to pressure fluctuations generated by the formation and dissipation of turbulent eddies or to processes related to the motion of particle clusters.

To determine whether the source mechanisms are primarily due to the eddies or the particle clusters, we analyze the energy distributions in the frequency domain of both the infrasound signal and the brightness signal extracted from high-speed camera images. Since these signals represent different physical quantities, a direct comparison of their magnitudes is inappropriate. Therefore, we normalize the signals by dividing each by its respective maximum value. Additionally, to perform baseline correction for variations in brightness within the intermittency zone, we subtract the average brightness value from the brightness signal (Figure 3a). The analysis concentrates on the time interval between 53 and 100 s, representing the simultaneous measurements taken within the intermittency zone.

When comparing the energy spectra of the cluster brightness to the infrasound signal, we observe many similarities (Figure 3b). Both cover the same frequency range, and they exhibit a very similar energy distribution, with the highest energy concentrations below approximately 4–5 Hz. Above this threshold, both energy spectra show a decay with a −5/3 slope, resembling the classical Kolmogorov energy cascade observed in turbulent flow (Figure 3b, black line) (Kolmogorov, 1941). The Kolmogorov energy cascade describes how turbulent kinetic energy transfers from larger to smaller scales in a fluid flow. The −5/3 slope in the frequency representation of the energy spectrum is a characteristic feature of turbulence, indicating the inertial subrange where energy is transferred without dissipation. Importantly, while Kolmogorov's theory primarily applies to velocity measurements, similar behavior is observed in directly related variables such as pressure (e.g., Brosch et al. (2021)).

This suggests that clusters at the location of the pylon are advected by the eddies of the turbulent energy cascade for frequencies above 5.8 Hz, and that infrasound is also generated by these same eddies within a similar frequency range, starting slightly earlier at 4.5 Hz. This small difference can be attributed to the larger spatial coverage of the infrasound measurements compared to the high-speed camera, which captures a broader range of eddies.

The energy spectra also provide an important indirect observation. The 5.8 and 4.5 Hz frequencies representing the onset of the energy cascades do not correspond to the largest eddy scale in the system. The typical largest eddy for these avalanches has a frequency of around 0.6 Hz (Brosch et al., 2021). Instead, both energy spectra deviate from the energy cascade already at 5.8 Hz/4.5 Hz, following a relatively flat and similar energy distribution at lower frequencies, with a few peaks showing direct correlation (e.g., inset in Figure 3b). The energy spectra indicate that these large-scale eddies are not associated with either clustering processes or infrasound generation and further support the idea of infrasound being related to clusters.

In summary, this comparison suggests that for higher frequencies (>4.5 Hz), infrasound is generated by small-scale eddies advecting particle clusters. Conversely, for lower frequencies, we suggest that large turbulent scales are not responsible for infrasound generation. At these lower frequencies, snow clusters may remain suspended due to various phenomena such as rapid injection of snow particles into the frontal region caused by excess pore pressure in the snow cover (Gauer & Issler, 2004), underpressure created by the avalanche on the airfield (Louge et al., 2011), abrupt expansion processes due to dispersive pressure caused by the collision between the dense basal layer and the topography, or internal collisions between avalanche surges (Köhler et al., 2016).

4.2. The Source Energy

Assuming that infrasound is generated by particle clusters simultaneously suspended within the intermittency layer, in a first approximation, we estimate the total infrasound energy, E_{t_0} (J), emitted by the clusters in

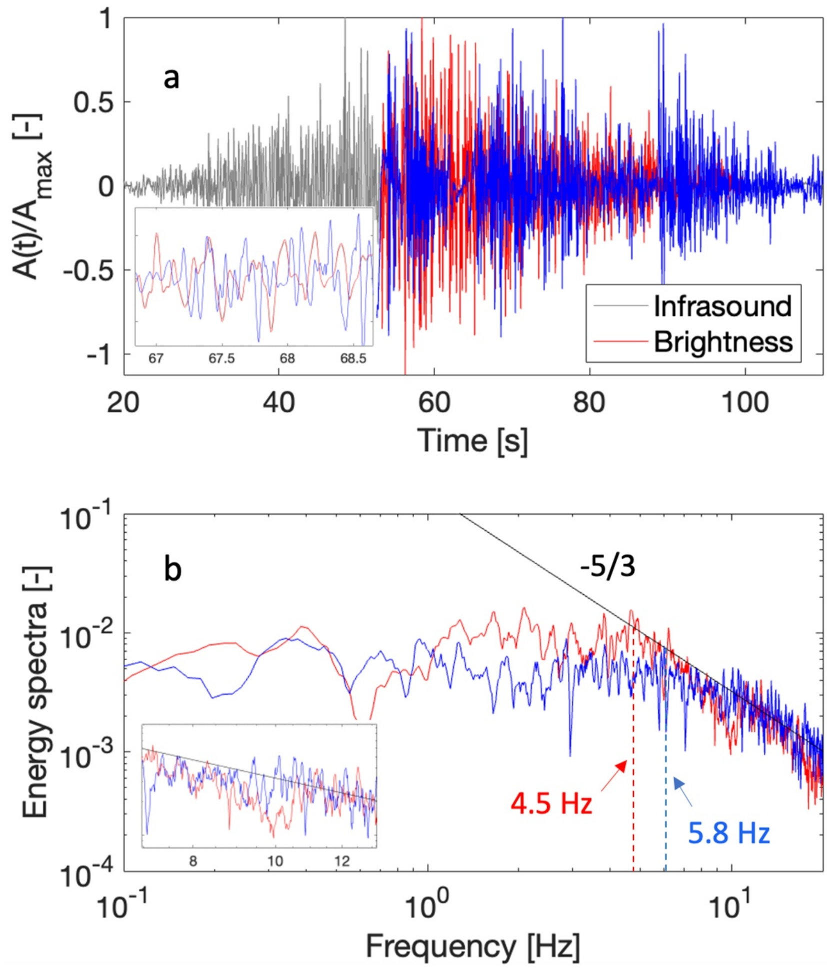

Figure 3. (a) Comparison of normalized infrasound (red and gray) and brightness (blue) signals. *A* denotes signal amplitude. The inset provides a zoomed view of the waveforms. (b) Energy spectra of the section of the same signals produced by the avalanche after reaching the pylon (colored portion of the signals in panel (a)). The black line in this spectrum represents the classical Kolmogorov energy cascade of the turbulent inertial range with a slope of −5/3. The vertical dashed lines at 4.5 and 5.8 Hz show the onset of the turbulent energy cascade for the infrasound and brightness data, respectively. The inset provides a zoomed view in the high-frequency range.

suspension following discussion presented at page 287 of Landau and Lifshitz (1987). The total infrasound intensity I_0 (W) radiated by an accelerating particle with radius R (m) that starts to move with a velocity u (m/s) is given by:

$$I_0(t) = \frac{8}{3}\pi\rho c R^2 u^2 e^{-\frac{2ct}{R}} \sin^2\left(\frac{ct}{R} - \frac{\pi}{4}\right) \tag{1}$$

where ρ (kg/m^3) is the air density, c is the speed of sound (331 m/s at 0 °C), and t (s) is time. The exponential term in Equation 1 acts to reduce the $I_0(t)$ almost immediately resulting in impulsive radiation that allows us to estimate the energy according to Landau and Lifshitz (1987) as:

$$E_0 = \frac{1}{3}\pi\rho R^3 u^2, \tag{2}$$

and is therefore proportional to the volume and squared velocity of the particle (Text S2 and Figure S5 in Supporting Information S1). Without considering interference effects between particles, the total infrasound energy (E_{t_0}) emitted by all particles (n) in suspension can be approximated as

19448007, 2025, 2, Downloaded from https://agupubs.onlinelibrary.wiley.com/doi/10.1029/2024GL112886 by CochraneAustria, Wiley Online Library on [13/01/2025]. See the Terms and Conditions (https://onlinelibrary.wiley.com/terms-and-conditions) on Wiley Online Library for rules of use; OA articles are governed by the applicable Creative Commons License

10.1029/2024GL112886

$$E_{t_0} = \sum_n \frac{1}{3}\pi\rho R_n^3 u_n^2. \tag{3}$$

The strong similarity between infrasound and kinetic energy of the particles in suspension E_p (J), both being proportional to particle volume and squared velocity, allows to define:

$$E_p = 2\frac{\rho_p}{\rho}E_{t_0}, \tag{4}$$

where ρ_p (kg/m^3) is the particle density. This simple derivation leads to the assumption that infrasound energy is proportional to the kinetic energy of the particle clusters in suspension. Consequently, since infrasound energy is proportional to the square of the velocity of the particles, the amplitude of the infrasound signal should increase with the velocity of the source.

4.3. The Source Distribution

The frequency analysis presented in Section 4.1 provides evidence suggesting that particle clusters in suspension are the source of the observed infrasound. According to Lindau's simplified model, described by Equations 1–3, the infrasound energy is proportional to the kinetic energy of these clusters (Equation 4), and thus the infrasound amplitude is proportional to their velocity. Consequently, we hypothesize that the total infrasound amplitude is proportional to the summation of all cluster contributions (proportional to velocity) acting simultaneously across the avalanche area, weighted by their respective distances to account for sound attenuation.

To verify this hypothesis and simultaneously understand the spatial distribution of the source, we can infer approximate locations and representative velocities of the particle clusters using Doppler radar measurements (Figure 4a). Their spatial distribution can be inferred under the assumption that clusters require sustained velocities to be ejected into the air or held in suspension by turbulence. In this study, we adopt a velocity threshold of 25 m/s as a reasonable lower limit for cluster formation (Sovilla et al., 2018). Regions in the avalanche, where a significant portion of the material flows faster than the velocity threshold, are identified using Doppler radar measurements, providing an approximate spatio-temporal representation of potential cluster activity (Figure 4b).

In this representation, each data point represents an area A of 25 m in length, corresponding to the Doppler radar range gate resolution, multiplied by the avalanche width W. The avalanche width is sketched in Figure 1 and is considered constant at $W = 150$ m. Finally, the material velocity V_{Imax} is considered representative of clusters belonging to each area A.

By assuming that the infrasound amplitude is proportional to the velocity of the clusters (Equation 2) and results from a linear combination of contributions from each area A (e.g., Johnson et al. (2021)), with each contribution being shifted according to acoustic propagation time, we can calculate the sum of all contributing sources at each time step $S(t)$ using the equation:

$$S(t) = \sum_{i=1}^{73} \frac{A V_{\mathrm{Imax}}(t - r_i/c)}{r_i}, \tag{5}$$

where the index i represents the 73 Doppler radar range gates and r_i (m) denotes the distance of each contributing area to the infrasound sensor.

Figure 4d shows the comparison of normalized root mean square (RMS) envelope of the infrasound signal, calculated over a 2-s running window (Figure 4c) and results of Equation 5. The curves are normalized for comparison and show good overall agreement. Notably, the correct timing of maximum amplitudes around 63 s is accurately captured, aligning with the maximum extension of the source spanning nearly 1-km behind the avalanche front and covering a significant portion of the entire avalanche path. The general increasing and decreasing trends are well captured, confirming the accurate assessment of the source distribution and the proportionality of infrasound amplitude to velocity. Figure S7 in Supporting Information S1 provides a sensitivity analysis in the calculation of $S(t)$ for varying velocity thresholds.

19448007, 2025, 2, Downloaded from https://agupubs.onlinelibrary.wiley.com/doi/10.1029/2024GL112886 by CochraneAustria, Wiley Online Library on [13/01/2025]. See the Terms and Conditions (https://onlinelibrary.wiley.com/terms-and-conditions) on Wiley Online Library for rules of use; OA articles are governed by the applicable Creative Commons License

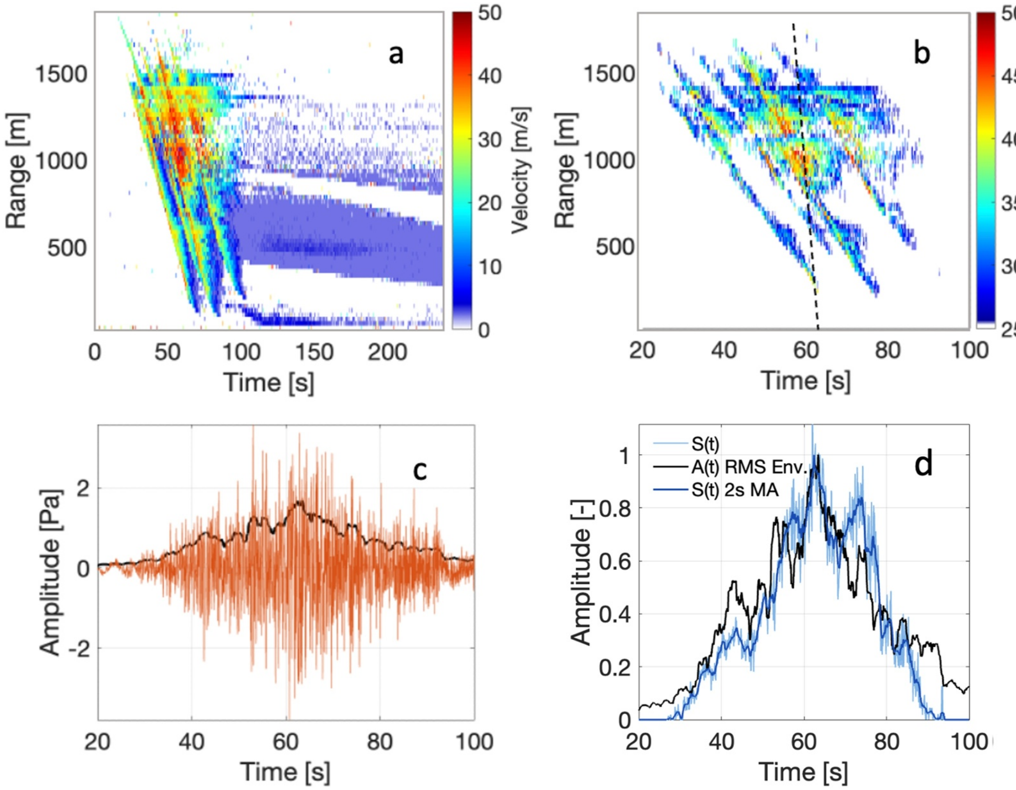

Figure 4. (a) Doppler radar velocities. (b) Spatio-temporal potential distribution of clusters derived from pixels with velocities exceeding 25 m/s in the Doppler radar measurements. (c) Infrasound signal emitted by the intermittency zone (red line), shown with its root mean square (RMS) envelope (black line). (d) Overlay of the sum of all contributing sources, $S(t)$ (Equation 5) and smoothing of $S(t)$ with a 2-s moving average, on the RMS envelope of the infrasound signal. The signals are normalized by their respective maximum values. The dashed line in panel (b) indicates the position of the sources that generate the maximum infrasound amplitude, according to acoustic propagation.

5. Conclusions

Our findings suggest that infrasound generated by PSAs primarily originates from clusters of suspended energetic particles, some of which are advected by small-scale turbulent eddies, while others are associated with non-turbulent processes. Furthermore, we propose that infrasound energy correlates with the square of the velocity and the volume of these particle clusters, implying that infrasound monitoring could serve as an indirect method to estimate a first-order magnitude of the kinetic energy of the suspended mass in PSAs, provided the cluster density (ρ_p) is known (Equation 4).

Our findings highlight that infrasound monitoring technologies are particularly effective in environments characterized by intense clustering activity, which typically occurs during cold snow conditions, leading to the formation of high-velocity and turbulent PSAs. This effectiveness is further enhanced in terrain where the topography of the avalanche path facilitates the expulsion of particles from the dense basal layer, including steep slopes, abrupt cliff faces, sudden changes in trajectory, and narrow gullies.

This new insight also provides a robust framework for explaining the exceptionally high infrasound levels observed in the plunging avalanche investigated by Watson et al. (2022) and the avalanche documented by Johnson et al. (2021), where the most intense infrasound emanated from a cliff band. In such conditions, the entire mass of the avalanche, including the slower-moving basal dense core, moves into suspension and undergoes acceleration under the influence of gravity, leading to a sudden surge in suspended particles and consequent kinetic energy. Conversely, the powder cloud may exhibit minimal sound activity, as noted in Johnson et al. (2021), when the suspended particles slow down and the cloud begins to settle.

19448007, 2025, 2, Downloaded from https://agupubs.onlinelibrary.wiley.com/doi/10.1029/2024GL112886 by CochraneAustria, Wiley Online Library on [13/01/2025]. See the Terms and Conditions (https://onlinelibrary.wiley.com/terms-and-conditions) on Wiley Online Library for rules of use; OA articles are governed by the applicable Creative Commons License

From a hazard mitigation perspective, correlating the kinetic energy of particle clusters with infrasound energy offers a new method to evaluate the destructive capability of PSA airborne layers. Indeed, airborne layers with higher energy levels can cause substantial runout and pose significant risks to protected areas with critical infrastructure, such as dams, which can be overrun by suspended materials.

Through the analysis of extensive infrasound data sets, such as those collected at VdlS, we could identify critical boundary conditions, such as snow cover or topography, that contribute to the formation of potent suspensions. In this regard, this study emphasizes the importance of conducting field campaigns or experiments to establish attenuation laws for infrasound propagation accounting for local topography, as well as the necessity of collecting complementary data on particle dynamics, such as employing an improved high-speed camera setup. Such advancements would enable more quantitative evaluation of the kinetic energy of the PSAs airborne layers and, finally, increase our ability to mitigate avalanche risk, with implications extending to similar phenomena like pyroclastic surges.

Data Availability Statement

The infrasound, Doppler radar, and GEODAR radar data utilized in this study are available on the ZENODO repository and can be accessed via the following link: https://doi.org/10.5281/zenodo.10966090 (Fischer et al., 2024). The brightness data are available at https://doi.org/10.5281/zenodo.10964650 (Kyburz & Sovilla, 2024).

Acknowledgments

The GEODAR and high-speed camera data were acquired as part of the Swiss National Science Foundation Grants 169640 and 143435, as well as support from the canton of Valais. The infrasound data were obtained through the CGL2017-84720-R project of the University of Barcelona, funded by the Spanish Ministry MINEICO-FEDER. We express gratitude to the UB Avalanche Team, particularly Pere Roig-Lafon, for their assistance in acquiring the infrasound data. Special acknowledgment is extended to our colleagues at the Electronics and Workshop departments of SLF for their invaluable support.

References

Ash, M., Chetty, K., Brennan, P., McElwaine, J., & Keylock, C. (2010). FMCW radar imaging of avalanche-like snow movements. In *2010 IEEE radar conference* (pp. 102–107). https://doi.org/10.1109/RADAR.2010.5494643

Bedard, A., Greene, G., Intrieri, J., & Rodriguez, R. (1988). On the feasibility and value of detecting and characterizing avalanches remotely by monitoring radiated sub-audible atmospheric sound at long distances.

Belli, G., Walter, F., McArdell, B., Gheri, D., & Marchetti, E. (2022). Infrasonic and seismic analysis of debris-flow events at illgraben (Switzerland): Relating signal features to flow parameters and to the seismo-acoustic source mechanism. *Journal of Geophysical Research: Earth Surface*, *127*(6), e2021JF006576. https://doi.org/10.1029/2021JF006576

Bernard, P. S., & Wallace, J. M. (2002). *Turbulent flow: Analysis, measurement, and prediction*. Wiley.

Brosch, E., Lube, G., Cerminara, M., Esposti-Ongaro, T., Breard, E. C. P., Dufek, J., et al. (2021). Destructiveness of pyroclastic surges controlled by turbulent fluctuations. *Nature Communications*, *12*(1), 7306. https://doi.org/10.1038/s41467-021-27517-9

Fischer, J.-T., Huguenin, P., Köhler, A., Pérez-Guillén, C., Suriñach, E., & Sovilla, B. (2024). Vallée de la Sionne Snow Avalanche n. 20213009: GEODAR radar, Doppler radar and infrasound data [Dataset]. *Zenodo*. https://doi.org/10.5281/zenodo.10966090

Gauer, P., & Issler, D. (2004). Possible erosion mechanisms in snow avalanches. *Annals of Glaciology*, *38*, 384–392. https://doi.org/10.3189/172756404781815068

Gauer, P., Kern, M., Kristensen, K., Lied, K., Rammer, L., & Schreiber, H. (2007). On pulsed Doppler radar measurements of avalanches and their implication to avalanche dynamics. *Cold Regions Science and Technology*, *50*(1), 55–71. https://doi.org/10.1016/j.coldregions.2007.03.009

Johnson, J. B., Anderson, J. F., Marshall, H. P., Havens, S., & Watson, L. M. (2021). Snow avalanche detection and source constraints made using a networked array of infrasound sensors. *Journal of Geophysical Research: Earth Surface*, *126*(3), e2020JF005741. https://doi.org/10.1029/2020JF005741

Kogelnig, A., Hübl, J., Suriñach, E., Vilajosana, I., & McArdell, B. W. (2014). Infrasound produced by debris flow: Propagation and frequency content evolution. *Natural Hazards*, *70*(3), 1713–1733. https://doi.org/10.1007/s11069-011-9741-8

Kogelnig, A., Suriñach, E., Vilajosana, I., Hübl, J., Sovilla, B., Hiller, M., & Dufour, F. (2011). On the complementariness of infrasound and seismic sensors for monitoring snow avalanches. *Natural Hazards and Earth System Sciences*, *11*(8), 2355–2370. https://doi.org/10.5194/nhess-11-2355-2011

Köhler, A., McElwaine, J. N., & Sovilla, B. (2018). GEODAR data and the flow regimes of snow avalanches. *Journal of Geophysical Research: Earth Surface*, *123*(6), 1272–1294. https://doi.org/10.1002/2017JF004375

Köhler, A., McElwaine, J. N., Sovilla, B., Ash, M., & Brennan, P. (2016). The dynamics of surges in the 3 February 2015 avalanches in Vallée de la Sionne. *Journal of Geophysical Research: Earth Surface*, *121*(11), 2192–2210. https://doi.org/10.1002/2016JF003887

Kolmogorov, A. N. (1941). The local structure of turbulence in incompressible viscous fluid for very large Reynolds. Numbers. *Doklady Akademii Nauk SSSR*, *30*, 301. https://doi.org/10.1098/rspa.1991.0075

Kyburz, M., & Sovilla, B. (2024). Vallée de la Sionne Snow Avalanche n. 20213009: High-speed camera recording and derived variables [Dataset]. *Zenodo*. https://doi.org/10.5281/zenodo.10964650

Landau, L. D., & Lifshitz, E. M. (1987). Fluid mechanics. In *(course of theoretical physics)* (2nd ed., Vol. 6). Butterworth-Heinemann.

Louge, M. Y., Carroll, C. S., & Turnbull, B. (2011). Role of pore pressure gradients in sustaining frontal particle entrainment in eruption currents: The case of powder snow avalanches. *Journal of Geophysical Research*, *116*(F4), F04030. https://doi.org/10.1029/2011JF002065

Marchetti, E., & Johnson, J. B. (2023). Infrasound array analysis of rapid mass movements in mountain regions. In *Advances in geophysics*. Elsevier. https://doi.org/10.1016/bs.agph.2023.06.001

Marchetti, E., van Herwijnen, A., Christen, M., Silengo, M. C., & Barfucci, G. (2020). Seismo-acoustic energy partitioning of a powder snow avalanche. *Earth Surface Dynamics*, *8*(2), 399–411. https://doi.org/10.5194/esurf-8-399-2020

Marchetti, E., Walter, F., & Meier, L. (2021). Broadband infrasound signal of a collapsing hanging glacier. *Geophysical Research Letters*, *48*(16), e2021GL093579. https://doi.org/10.1029/2021GL093579

McKenna, M. H., Gibson, R. G., Walker, B. E., McKenna, J., Winslow, N. W., & Kofford, A. S. (2012). Topographic effects on infrasound propagation. *Journal of the Acoustical Society of America*, *131*(1), 35–46. https://doi.org/10.1121/1.3664099

19448007, 2025, 2, Downloaded from https://agupubs.onlinelibrary.wiley.com/doi/10.1029/2024GL112886 by CochraneAustria, Wiley Online Library on [13/01/2025]. See the Terms and Conditions (https://onlinelibrary.wiley.com/terms-and-conditions) on Wiley Online Library for rules of use; OA articles are governed by the applicable Creative Commons License

Naugolnykh, K., & Bedard, A. (2002). A model of the avalanche infrasonic radiation. In *IEEE international geoscience and remote sensing symposium* (Vol. 2, pp. 871–872). https://doi.org/10.1109/IGARSS.2002.1025713

Sovilla, B., McElwaine, J. N., & Köhler, A. (2018). The intermittency regions of powder snow avalanches. *Journal of Geophysical Research: Earth Surface*, *123*(10), 2525–2545. https://doi.org/10.1029/2018JF004678

Watson, L. M., Carpenter, B., Thompson, K., & Johnson, J. B. (2022). Using local infrasound arrays to detect plunging snow avalanches along the Milford Road, New Zealand (Aotearoa). *Natural Hazards*, *111*(1), 949–972. https://doi.org/10.1007/s11069-021-05086-w

19448007, 2025, 2, Downloaded from https://agupubs.onlinelibrary.wiley.com/doi/10.1029/2024GL112886 by CochraneAustria, Wiley Online Library on [13/01/2025]. See the Terms and Conditions (https://onlinelibrary.wiley.com/terms-and-conditions) on Wiley Online Library for rules of use; OA articles are governed by the applicable Creative Commons License